

CALCULATIONS OF TECTONIC, MAGMATIC AND RESIDUAL STRESS IN THE ŠTIAVNICA STRATOVOLCANO, WESTERN CARPATHIANS: IMPLICATIONS FOR MINERAL PRECIPITATION PATHS

MICHAL NEMČOK^{1a,b*}, PATRIK KONEČNÝ^{1a} and ONDREJ LEXA²

^{1a}Slovak Geological Survey, Mlynská dolina 1, 817 04 Bratislava, Slovak Republic

^{1b}Department of Geology and Paleontology, University of Salzburg, Hellbrunner Strasse 34, 5010 Salzburg, Austria

²Department of Petrology, Charles University, Albertov 6, 128 43 Prague, Czech Republic

(Manuscript received September 1, 1998; accepted in revised form September 28, 1999)

Abstract: This paper describes the dynamics controlling the development of the Štiavnica stratovolcano and the distribution of related ore deposits during the Badenian–Pannonian (16.5–6.2 Ma) using combined structural, geobarometric and geothermometric analyses. During the early Badenian–earlier late Badenian (16.5–15 Ma) the Štiavnica area experienced NE–SW extension. It controlled NW–SE striking normal- and N–S trending sinistral strike-slip faults. Later, during the early Badenian–earlier late Badenian, the extension rotated to W–E and controlled N–S striking normal faults, NE–SW striking sinistral and NW–SE striking dextral strike-slip faults. Later, the extension rotated to NW–SE. The tectonic stress interacted with the rapid overburden removal and magmatic stress of the granodiorite intrusion, during the late Badenian–early Sarmatian. The tectonic stress controlled NE–SW trending normal faults. Overburden reduction input changed normal faulting to strike-slip faulting. Magmatic input caused the opening of subhorizontal veins above the intrusion and anastomosing fracture pattern around its boundary. Later during the late Badenian–early Sarmatian, the stress had a plane stress character ($\sigma_1 > \sigma_2 > \sigma_3$), indicating neither collapse nor distinct regional extension. NE–SW striking normal faults, ENE–WSW striking sinistral and N–S striking dextral strike-slip faults were active. Normal faults and releasing bends of the strike-slip faults were places of ore deposit precipitation. During the Sarmatian–Pannonian (13.6–10.7 Ma), the stress progressively gained a strong oblate character ($\sigma_1 \geq \sigma_2 \gg \sigma_3$), indicating strong regional NW–SE extension, controlling the same fault pattern. Later during the Pannonian, counterclockwise stress rotation towards N–S oriented σ_1 and E–W oriented σ_2 led to NE–SW oriented sinistral strike-slip faulting.

Key words: Western Carpathians, Štiavnica stratovolcano, stress, temperature, fault, vein.

Introduction

During the Miocene, the Carpathian orogen migrated towards the NE and E, synchronously with the subduction of the remnant Carpathian Flysch Basin, underlain by an oceanic/paraoceanic crust and located between the overriding Carpathians and European platform. This migration ceased when the Carpathians made contact with the passive margin of the European Platform (e.g. Royden & Baldi 1988) and subduction stopped. Another control of the Carpathian development was the eastward lateral extrusion of the Eastern Alps after the Apulia–Europe collision (e.g. Ratschbacher et al. 1991a,b; Csontos et al. 1992). The shortening in the frontal, accretionary, parts of the Carpathians and subduction rollback were compensated by the intra- and back-arc extension, accompanied by the asthenosphere elevation in the back-arc region (e.g. Royden et al. 1982, 1983a,b; Bergerat 1989; Stegena et al. 1975). This geotectonic situation and the distribution of the old continental crust in the Inner Carpathians controlled the space- and time distribution and composition of the Miocene–Quaternary Carpathian volcanism (Lexa et al. 1993).

The temporal development of the Štiavnica stratovolcano (Fig. 1) is as follows (Lexa et al. 1999; Mafo et al. 1996;

Konečný et al. 1983; Konečný & Lexa 1984; Kantor & Ďurkovičová 1985; Kantor et al. 1988).

The stratovolcano started to form during the early Badenian (16.5–15.5 Ma) (Fig. 2a), built by pyroxene/hornblende-pyroxene andesite lava flows, extrusive domes, pyroclastic flow deposits and epiclastic breccias. Andesite/andesite porphyry sills and lacoliths were emplaced in its central and basal parts. Related alterations comprised chloritization and hematitization of intrusions. The stratovolcano then underwent denudation roughly synchronous with emplacement of the quartz-diorite body in its center during the Badenian–early Sarmatian (16.5–12.7 Ma) (Fig. 2b).

During the late Badenian–early Sarmatian (15–12.7 Ma), activity of the high sulphidation fluids began causing the argillitic alteration of host rocks and mesothermal mineralizing events. Denudation of the stratovolcano further continued roughly synchronous with the emplacement of the large granodiorite intrusion (Fig. 2c). The intrusion, which had flat roof and outward dipping margins, was situated in the crystalline basement and its Mesozoic sedimentary cover. A number of related porphyritic granodiorite apophyses were emplaced into the Mesozoic rocks. At the contact of the granodiorite and the Mesozoic carbonates, magnetite skarns were formed. Local fluids in the upper central parts of the

*Present address: Energy and Geoscience Institute, University of Utah, 423 Wakara Way, Salt Lake City, UT 84108, USA;
mnemcok@egi.utah.edu

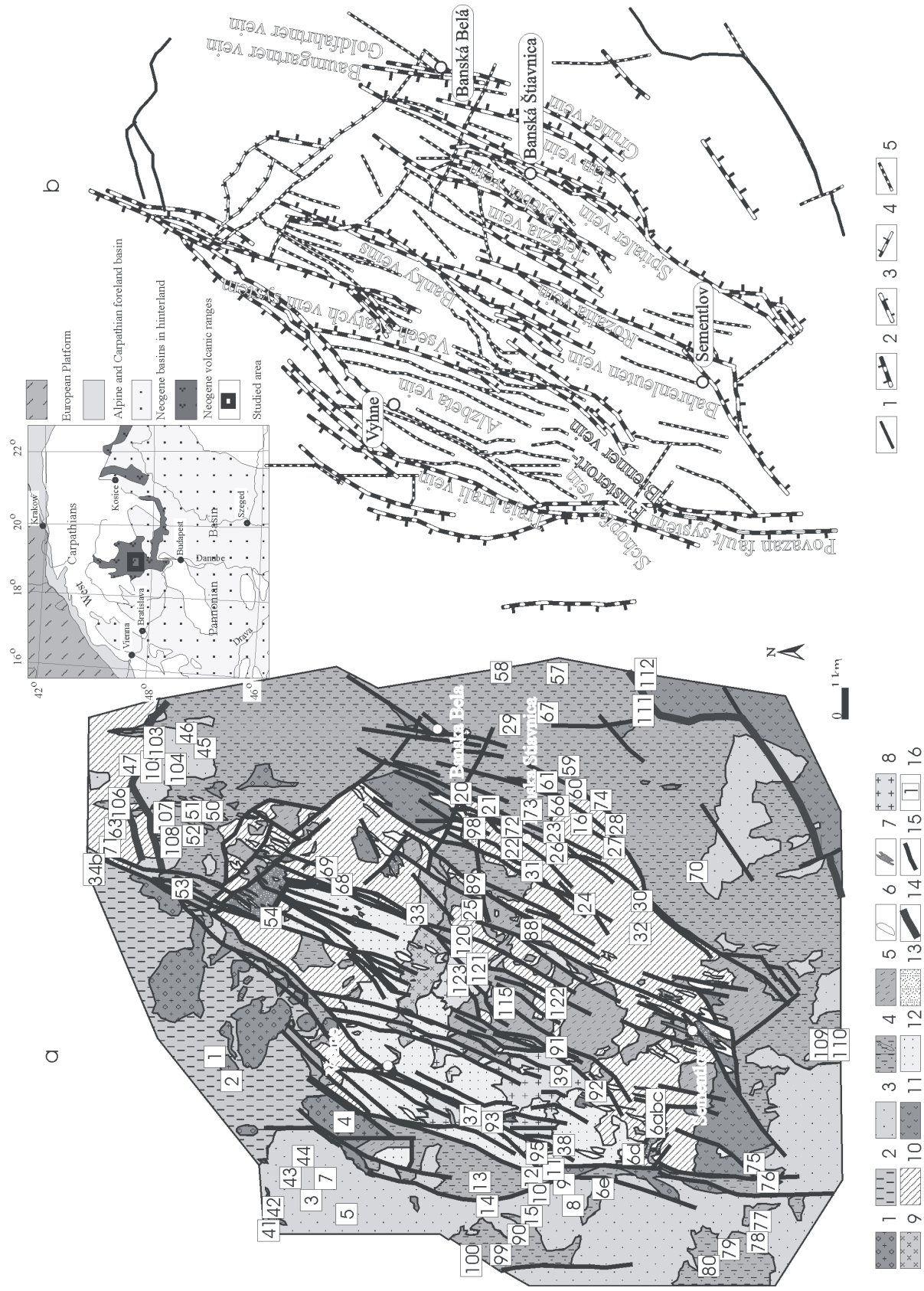


Fig. 1. Text on the next page.

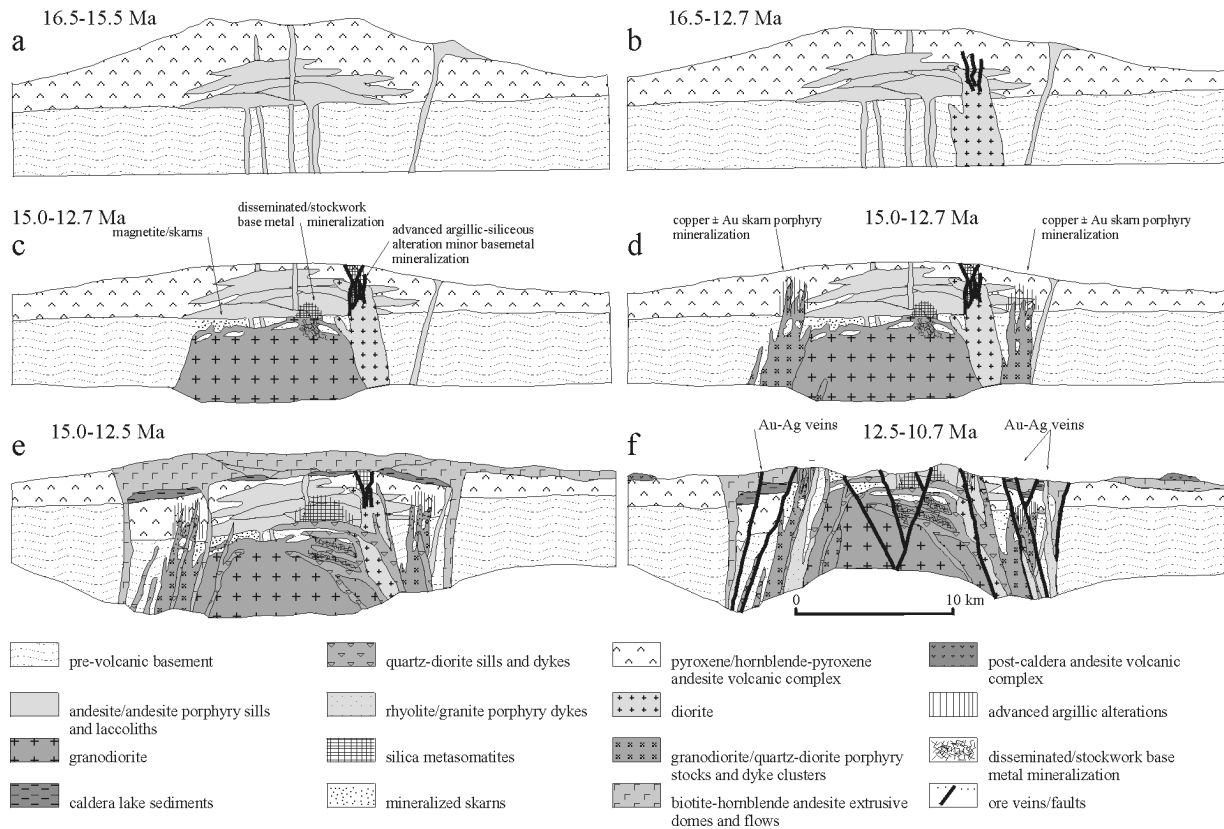


Fig. 2. Cartoon of the development of the Štiavnica stratovolcano from 16.5 to 10.5 Ma (after Lexa et al. 1999). Explanation in text.

granodiorite intrusion and surrounding andesite led to the formation of the stockwork base metal mineralization accompanied by quartz, pyrite, pyrophyllite and kaolinite alterations. δD values of inclusion fluids in the quartz and sphalerite ranging from -52 to -67 ‰ SMOW, about -75 ‰ in chlorite and kaolinite; isotopic composition of the Pb-rich

ores ($^{206}\text{Pb}/^{204}\text{Pb} = 18.810\text{--}18.839$, $^{207}\text{Pb}/^{204}\text{Pb} = 15.659\text{--}15.682$, $^{208}\text{Pb}/^{204}\text{Pb} = 38.922\text{--}39.011$) indicate an important role of magma-derived fluids (Háber et al. 1997). Later on, during the continuing denudation of the stratovolcano, granodiorite/quartz diorite porphyry stocks and dyke clusters were emplaced around the granodiorite intrusion (Fig. 2d). Some of the dykes penetrated by bore hole B-1 (Fig. 3) were re-opened either through their median lines or along their margins (Štöhl et al. 1990a). Fluids related to different stocks/dyke clusters gave rise to copper porphyry/skarn ore deposits and host rock alterations.

Later, during the late Badenian–early Sarmatian (15–12.7 Ma), it has been postulated that a caldera was formed (Konečný & Lexa 1984), filled by sediments, reworked tuffs, biotite-hornblende andesite/dacite extrusive domes, dome flows and pyroclastic flows and was accompanied by the emplacement of quartz-diorite porphyry sills and dykes (Fig. 2e).

During the Sarmatian (13.6–11.5 Ma), andesitic volcanic activity from dispersed centers on the slopes of the stratovolcano revived and the uplift of the horst structure in the central parts began (Fig. 2f). The continuing uplift was accompanied by the emplacement of rhyolitic and granite porphyry bodies along the horst boundary faults, during the late Sarmatian–early Pannonian (12–10.7 Ma). Low sulphidation fluids gave rise to base and precious metal vein-type mineralization and adularia, sericite alterations. K/Ar ages of 12.3–13.3 Ma (± 0.4 – ± 1.2) from various sericite samples constrain the time of this ore deposition (Tschernyshev et al. 1995). δD values of inclusion fluids in the quartz, baryte

Fig. 1. a) Structural scheme of the central zone of the Štiavnica stratovolcano (after Štöhl et al. 1990b) with localities of kinematic data collection and fault pattern. 1 — rhyolite dyke and extrusive dome, upper Sarmatian–lower Pannonian; 2 — rhyolite volcanoclastic rock, upper Sarmatian–lower Pannonian; 3 — post-caldera andesite and volcanoclastic rock, Sarmatian; 4 — hornblende-biotite andesite caldera filling and hornblende-biotite andesite porphyry-dyke, upper Badenian–lower Sarmatian; 5 — quartz-diorite porphyry—sill, upper Badenian–lower Sarmatian; 6 — quartz-diorite porphyry—dyke, upper Badenian–lower Sarmatian; 7 — cluster of dykes and stock of granodiorite porphyry, upper Badenian–lower Sarmatian; 8 — granodiorite, Badenian–lower Sarmatian; 9 — diorite, Badenian–lower Sarmatian; 10 — pre-caldera propylitized andesite, Badenian; 11 — pre-caldera andesite and volcanoclastic rock, Badenian; 12 — pre-volcanic basement, Carboniferous–Karpatian; 13 — secondary quartzite, upper Badenian–lower Sarmatian; 14 — caldera marginal fault; 15 — fault; 16 — locality. **b)** Main structures with ore deposits with original names. 1 — caldera marginal fault, 2 — NW-dipping fault, 3 — SE-dipping fault, 4 — NE-dipping fault, 5 — subvertical fault. Note the use of „classical“ vein names, used traditionally but incorrectly for ore deposit bodies formed along normal and strike-slip faults.

1984). This does not mean that separated tectonic events overlap, only that their limits are understood as broader boundaries.

In order to determine the angle of the internal friction and cohesion for the reduced stress tensor calculation and the σ_1 , σ_3 stress relationship for the calculation of stress magnitudes, the rock mechanics tests have been carried out on granodiorite samples. The samples were cylindrical, 3.78 cm in diameter and 5.75–5.98 cm in height.

The principal stress magnitudes were computed applying the following equations of Angelier (1989):

$$\psi = \sigma_3/\sigma_1 \quad (1)$$

$$R = (\sigma_2 - \sigma_3)/(\sigma_1 - \sigma_3) \quad (2)$$

$$\sigma_1 = \sigma_v \quad (3)$$

where R is a stress ratio, calculated by the Hardcastle & Hills (1991) method. For a given lithology, the σ_3/σ_1 ratio (ψ) was derived from the Mohr circle envelope graph. The Mohr envelope was constructed as a line inclined to the x axis (normal stress) at the angle of internal friction, and cutting the y axis (shear stress) at the value of cohesion. For normal faulting, the value for σ_1 equalled the overburden load σ_v , which is given by ρgh , where ρ is the density of stratovolcanic rocks, g the acceleration of gravity (rounded to 9.812 ms^{-2}), and h the thickness of overburden. This thickness was given by the height of the stratovolcanic cone, reconstructed on the basis of inclinations of preserved lava and pyroclastic flows, and estimated at about 3000 m (V. Konečný & J. Lexa 1995, pers. commun.). The central parts of the missing stratovolcanic cone were built by intrusive rocks, lava flows and minimally by volcanoclastics (15–20 %; V. Konečný 1996; pers. commun.). The density of the volcanic basement composed dominantly of calcic dolomite is $2750\text{--}2850 \text{ kgm}^{-3}$, density of andesite $2500\text{--}2600 \text{ kgm}^{-3}$, density of volcanoclastics $2000\text{--}2200 \text{ kgm}^{-3}$, density of quartz-diorite porphyry 2630 kgm^{-3} , density of diorite porphyry 2630 kgm^{-3} , density of diorite 2680 kgm^{-3} and density of granodiorite 2640 kgm^{-3} (Šefara et al. 1976; Ibrmajer et al. 1989). The mineralogical densities, corrected for porosity, are 2700 kgm^{-3} for quartz-diorite porphyry, 2680 kgm^{-3} for diorite porphyry, 2730 kgm^{-3} for diorite and 2710 kgm^{-3} for granodiorite. σ_2 was calculated by combining equations 1 to 3: $\sigma_2 = \sigma_v (R + \psi - R\psi)$, where R, determined from reduced stress calculation, is 0.4 and ψ , determined from Mohr circle envelope graph (Fig. 4), is 0.0062893.

Having calculated the principal stress magnitudes of the tectonic stress, the interplay of the tectonic stress, overburden removal and magmatically induced stress was studied. Increments of overburden removal by erosion were directly subtracted from the σ_1 value. Vertical magmatic stress, calculated by buoyancy equation (e.g. Price & Cosgrove 1991), was also subtracted directly from σ_1 . Subtractions of load and magmatic pressures from σ_2 and σ_3 were equal to $v/(\rho gh(1-v))$ following Jaeger & Cook (1976), where v is Poisson's ratio, ρ is the density, g is the acceleration of gravity and h is the depth. Calculations, which used magmatic

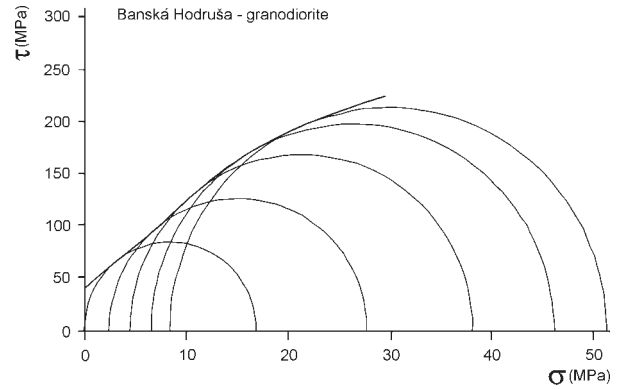


Fig. 4. Mohr-circle envelope determined by triaxial testing of the upper Badenian-lower Sarmatian granodiorite. The determined cohesion is 38.9 MPa, the angle of internal friction varies from 40 to 20°, depending on the confining pressure.

stress, were also made to test the values provided by geobarometric and geothermometric study, the precision of which is at the limits of the applied methods.

The effect of the temperature change, related to the overburden removal, on the development of the residual stress was calculated from the equation following Suppe (1985):

$$\Delta\sigma_r = [\alpha E/(1-\nu)] * (dT/dz)\Delta z \quad (4)$$

where $\alpha = 7 \cdot 10^{-6} \text{ }^\circ\text{C}^{-1}$ is the linear thermal expansion coefficient, E is the Young's modulus, dT/dz is the thermal gradient and Δz is the change in depth. The volume change was calculated from:

$$\alpha dT = v/(100-\nu) \quad (5)$$

where v is the volume change of the intrusion in %.

The T-t path modeling of the contact aureole of the granodiorite intrusion was made by the software of Peacock (1990), using an explicit finite difference algorithm to solve the one-dimensional heat transfer problem. Granodioritic magma was assumed to be intruded instantaneously, at temperature $750 \text{ }^\circ\text{C}$ (own data) and crystallized over a $100 \text{ }^\circ\text{C}$ temperature interval. Other assumptions for the modeling are: during crystallization, the magma released 100 kJkg^{-1} , the temperature of the country rock was $100 \text{ }^\circ\text{C}$, the width of the intrusion is 5 km, the thermal conductivity was $2.75 \text{ Wm}^{-1}\text{K}$ (taken from Cermak & Rybach 1982), the heat capacity was $1050 \text{ Jkg}^{-1}\text{K}$ (taken from Cloetingh et al. 1995). Following the T-t path modeling, the temperature gradient that develops the cooling-related residual strength higher than the tensional strength of the granodiorite/andesite was calculated from:

$$\Delta T > [\sigma_t(1-\nu)]/\alpha E \quad (6)$$

where σ_t is the tensional strength. Fracturation events were determined at each point of T-t cooling paths where the tensional strength of the rock was overcome.

In order to determine the magmatic pressures in the magma chamber and in the upper parts of the granodiorite intrusion and the depths of the chamber and top of the intrusion,

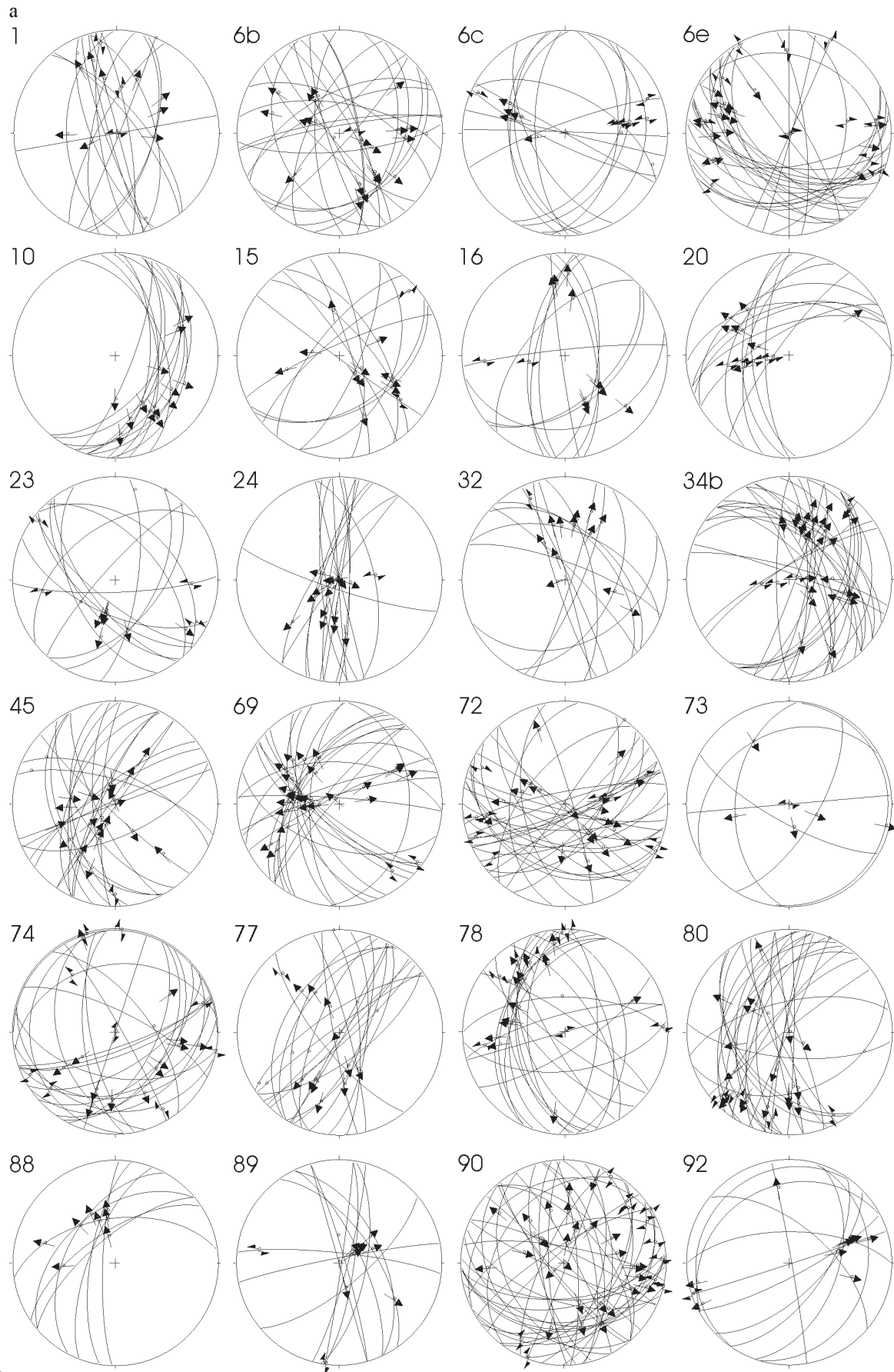


Fig. 5a.



geobarometric and geothermometric analyses of granodiorite samples were made. Unpublished data of Konečný (1996, pers. commun.), made by projections of volcanic structures in cross-sections, were used to correct the data on top of the intrusion. These data together were used for the calculation of the tectonic and magmatic stress interplay. Mineral phases were analyzed using a JEOL-733 microprobe. A set of natural and synthetic (pure oxide) standards were used for the calibration. The operating conditions were: accelerating voltage 15 kV, probe current 20 nA and counting time 20 s. Points in the amphibole were placed within the central parts

The application of geobarometer required several conditions to be met. The mineral assemblage, besides amphibole, must involve the following phases: biotite, plagioclase, orthoclase, quartz, magnetite and titanite. Oxygen fugacity should have no effect on amphibole composition because it is buffered by the magnetite-ilmenite pair. Pure water (no CO₂) is supposed to constitute a fluid phase. Only the rims of amphiboles should be analyzed to obtain a narrow interval of pressures during the final crystallization.

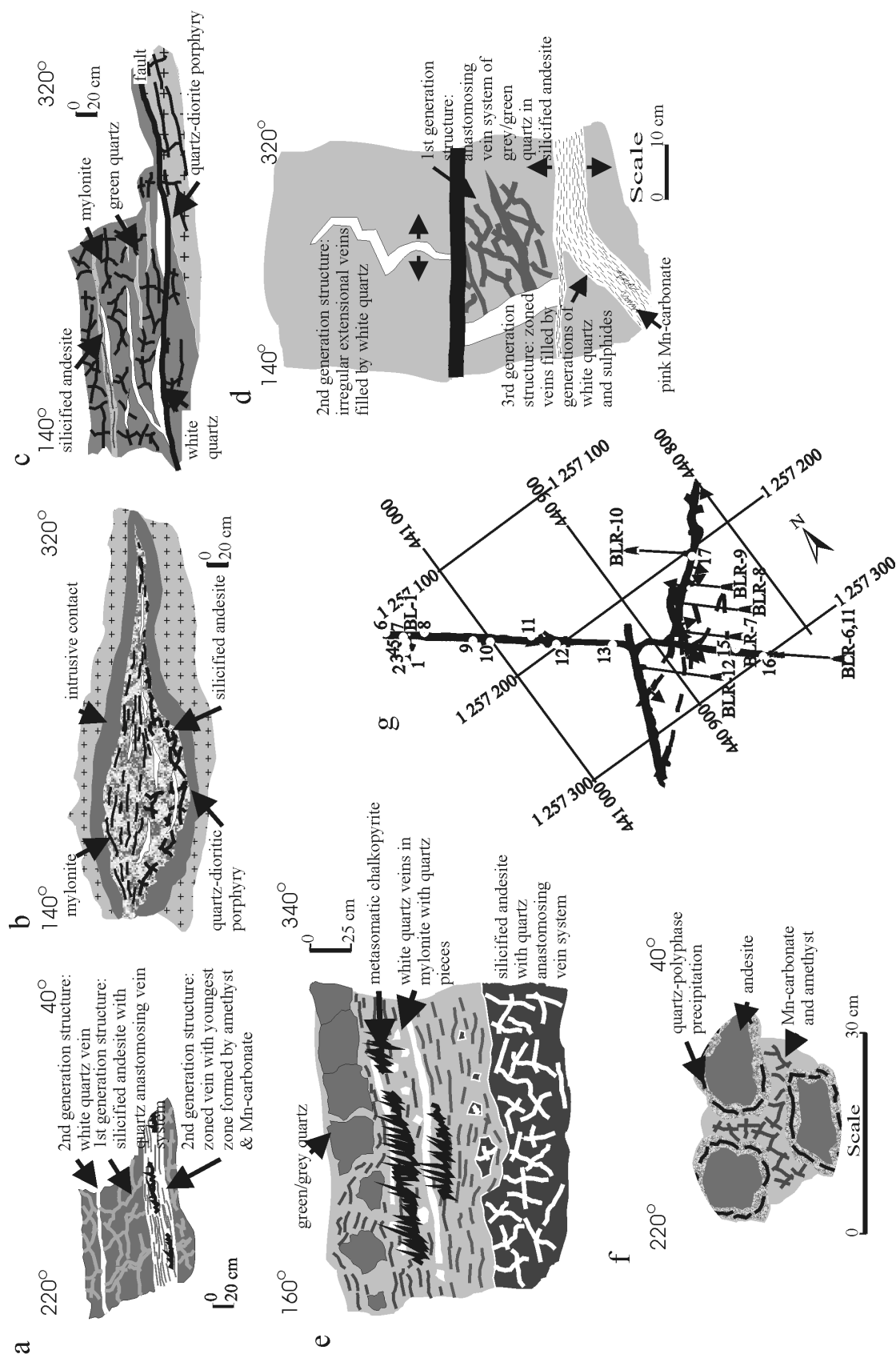


Fig. 6. (a–f) Cross-cutting relationships of various structures at localities of the Rozália Mine 14th floor in Banská Hodruša. The 14th floor is located in Fig. 3. Field sketches a–f were made at sites localized in Fig. 6g: 2, 7, 12, 1, 4, 3. (g) 14th floor of the Rozália Mine with localities of kinematic data collection. The grid is in meters, localities are numbered and codes indicate bore holes. Locations are different from surface locations in Fig. 1.

Data

The data comprise fault-striae, extension vein readings (Fig. 5) and granodiorite sample analyzes.

Most of the extensional veins are filled by idiomorphic minerals (stretched type sensu Ramsay & Huber 1983) originated by elastic fracturation accompanied by insufficient fluid flow. This type indicates only a rough direction of σ_3 , parallel to their opening vector, assumed to be perpendicular to vein walls. Stretched-type veins are not present in the Sarmatian andesites, rare in upper Sarmatian-lower Pannonian rocks (only at location 4 with NW-SE strikes), frequent in upper Badenian-lower Sarmatian rocks (locations 6e, 33, 39a, 72, 98 with usually NE-SW oriented veins) and abundant in lower Badenian-early upper Badenian rocks (locations 6a, b, c, 16, 20, 22, 24b, 34b, 35, 47, 74, 75b, 87 with dominantly NE-SW oriented and subordinate NW-SE veins). The only fibrous veins, which indicate opening with sufficient fluid flow, and which indicate the opening vector exactly, are present at location 87 (Badenian rocks) and along the Rozália vein (Figs. 1, 3) having W-E to WNW-ESE oriented fibers (parallel to σ_3).

All faults were formed and/or reactivated in the brittle environment, with the exception of narrow zones, which underwent a temporal ductile regime due to the thermal and chemical activity of migrating fluids. Faults along the NW and SE side of the central Štiavnica zone dip to the NW and SE, respectively (Figs. 1, 3). The central zone itself is deformed by a complicated fault pattern containing faults with NW, SE and vertical dips. Meso-scopical faults from locations are shown in Fig. 5.

The cross-cutting relationships of various structures in the field indicate that the oldest fracture pattern is formed by the anastomosing vein pattern, the network of small fractures with quartz fill, without any preferred orientation (Fig. 6a-e). It is accompanied by quartz, pyrite, pyrophyllite and kaolinite alterations. The anastomosing vein system is cross-cut by a subhorizontal system of quartz and carbonate veins (Fig. 6a-c), called the Svetozár vein system (sensu Mafo et al. 1996). Some of them show evidence of cycles of increased fluid pressure (Fig. 6f), indicated by repeated episodes of hydraulic fracturing. Fig. 6f indicates that the andesite host rock was opened by hydraulic fracturing. Fracture patterns were conduits for fluids, which migrated away from the area of the fluid overpressure and caused its decrease. Decreased fluid pressure triggered mineral precipitation, which sealed rock fragments in precipitated quartz fill (Fig. 6f). Sealing of the escape paths caused a second cycle of the overpressure that triggered the second fracturation event. It is indicated by pieces of rock lined by quartz fill that remained in precipitated Mn-carbonate and amethyst fill (Fig. 6f). Sometimes subvertical quartz veins opened by W-E extension cross-cut the pre-existing subhorizontal quartz and carbonate vein system and are cross-cut by younger subhorizontal quartz-sulphidic vein system (Fig. 6d). All these structures are older than the quartz diorite porphyry sills and dykes. This is indicated by the intrusive contact of the quartz-diorite porphyry with pre-existing silicified andesite deformed by the anastomosing vein sys-

tem and subhorizontal (Svetozár system-type sensu Mafo et al. 1996) veins (Fig. 6b,c). The relationship of the various petrographic rock types in dykes indicates multiple intrusion from differentiated magma chamber. All above mentioned structures are deformed by the NE-SW normal faults. The dip of normal faults varies between 50° and 90°. They are connected by subhorizontal detachments, as is documented in a few cases (Fig. 6c-e). Subhorizontal detachments frequently formed along earlier subhorizontal veins, causing their boudinage in zones wrapped in mylonite (Fig. 6e).

Two samples were taken from the central part of the granodiorite body, with a coarse granular texture. One was collected from the bore hole (B1/1368) and the other one from the outcrop. Both samples do not indicate any alteration. Granodiorite consists of plagioclase, orthoclase, amphibole, biotite, quartz and Fe-Ti oxides. Some euhedral minerals of plagioclase have zone of resorption near their rims. Intensive resorption edges are present in amphiboles, less in biotites, indicating that the magma was not oversaturated with water (only 2–5 %).

The parameters of the granodiorite determined by the rock mechanics tests (Fig. 4) are as follows: tensional strength = 2.5–4.9 MPa, cohesion = 38.9 MPa, angle of the internal friction = 40–20°, Young's modulus = $6.5 \cdot 10^4$ MPa, Poisson's ratio = 0.22. It has to be said that the tensional strength of the granodiorite is very low due to its alteration. That is why the fresh-rock value of 20 MPa (taken from Suppe 1985) was used for the modeling of fracturation developed by the residual stress due to cooling.

Results

Amphibole and plagioclase from granodiorite samples are mineral phases, which crystallized in the early stages of solidification of granodiorite and hence yield information regarding physical conditions in the magma chamber. Dependence of the aluminium content on pressure has been used for the formulation of the amphibole geobarometer (Hammarstrom & Zen 1986; Hollister et al. 1987; Johnson & Rutherford 1988; Schmidt 1992; Anderson & Smith 1995). Amphibole barometer application was limited by several conditions. The mineral assemblage had to involve all nine mineral phases: amphibole, biotite, plagioclase, orthoclase, quartz, magnetite and titanite. Štiavnica granodiorite is pure on titanite which otherwise has a negligible impact on amphibole composition. The anorthite content in plagioclase outer zones should be in the range An_{35} – An_{25} . The basicity of studied plagioclases apparently decreases from core to rim from An_{60} to An_{32} . The role of iron and its ferric/ferrous ratio is fundamentally important. More reduced amphiboles with $Fe^{3+}/(Fe^{3+}+Fe^{2+})$ less than 0.25 were not utilized as well as $Fe_{tot}/(Fe_{tot}+Mg)$ outside the 0.4–0.65 range. Using the equation of Anderson & Smith (1995) and an average temperature of about 730 °C, the pressures were found to range from 1.5 to 4.1 kbar with average 2.8 kbar (18 estimations).

Assuming that the total pressure equals the fluid pressure in a fluid saturated system, the depth of the magma chamber was estimated. In the case of the Štiavnica granodiorite, the

system did not achieve a fluid saturated state, indicated, for example, by resorption of phenocrysts in the late stages of crystallization. The probable magma chamber is estimated to be located at depths greater than 10 km. The essential part of the magma chamber passively intruded to a level about 2.5 km below the surface including the eroded cover (V. Konečný & J. Lexa 1999, pers. commun.), determined by cross-section restoration.

Temperatures in the magma chamber have been evaluated using the amphibole-plagioclase semi-empirical geothermometer of Blundy & Holland (1990). The use of this geothermometer places some limitations on the composition of the mineral phases. Amphiboles cannot exceed 7.8 silica atoms pfu and the plagioclases must be less calcic than An_{92} . This thermometer is valid over the temperature range 500–1100 °C with deviation of around 75 °C. The fundamental condition is to determine equilibrium pairs. The anorthite content of plagioclases decreases more or less from core to rim. Small euhedral plagioclases around An_{65} – An_{68} are often enclosed in amphiboles which crystallized together with amphiboles. Calculated equilibrium temperatures range from 690 to 790 °C, indicating crystallization above water saturated granitoid solidus (≈ 700 °C, Piwinski 1975).

The calculated paleostress configurations were separated into four groups representing four tectonic regimes during the: early Badenian–earlier late Badenian (16.5–15 Ma), late Badenian–early Sarmatian (15–12.7 Ma), Sarmatian (13.6–11.5 Ma) and late Sarmatian–early Pannonian (12–10.7 Ma) (Table 1). The limits of several of these periods overlap, which is a consequence of the overlapping ages of the studied rocks.

The early Badenian–earlier late Badenian (16.5–15 Ma) period was characterized by stress changes, that is clockwise rotation of the maximum horizontal stress. NE–SW oriented extension acted at the beginning of this period (Fig. 7). Evidence of its activity is recorded at locations 6d, 23, 64 and 72 (Table 1). The stress configuration is characterized by the oblate stress ellipsoid ($\sigma_1 \geq \sigma_2 > \sigma_3$). The magnitude of σ_2 was similar to σ_1 and the magnitude of σ_3 was distinctly lower than σ_2 and σ_1 . This caused a distinct regional extension driven by the active subduction in front of the Carpathians to the NE of the Štiavica region (Jiríček 1979; Książkiewicz 1960; Vialov 1974). Subvertically oriented σ_1 and NW–SE σ_2 had close enough magnitudes to experience the σ_2/σ_1 exchange in the case of regional stress pulses and/or the subtraction of the overburden load. Regional stress pulses or the regional stress interplay with varying vertical forces occasionally activated strike-slip faulting, (e.g. evidence at location 47, Table 1). Varying vertical forces were caused by episodes of magma emplacement (Fig. 2) and/or geologically fast changes of the stratovolcanic relief, that is fast development of volcanic cones and fast selective erosion.

Later, during the early Badenian–earlier late Badenian, both mentioned stress configurations, with NE–SW oriented extension, progressively rotated towards the configuration with W–E oriented σ_3 and subvertical σ_1 (Fig. 7). Evidence of such a changed stress is present at locations 6c, 27, 30, 55, 84b, 84d and 109 (Table 1). Calculated stress ellipsoids from data allowing the use of the Hardcastle & Hills (1991) meth-

od have either an oblate (sites 6c, 55) or prolate character ($\sigma_1 > \sigma_2 \geq \sigma_3$) (site 109). At the end of the early Badenian–earlier late Badenian period, the stress field further rotated clockwise towards the position with NW–SE oriented σ_3 and subvertical σ_1 (Fig. 7). Evidence of its activity is recorded at locations 6a, 24a, 27, 68, 74, 75, 88a, 107 (Table 1). Stress ellipsoids determined from locations 74, 88a and 107 have prolate shapes. Pulses of the regional stress or its interplay with varying vertical forces caused the σ_2/σ_1 exchange and occasionally activated strike-slip faulting, (e.g. evidence at location 71).

Fig. 7 shows which faults were active during the early Badenian–earlier late Badenian. To discuss its value, we emphasize that the activity of faults is indicated by field evidence and non activity is indicated by lack of evidence. This means that, despite the study of all suitable outcrops along faults in Fig. 7, the small chance remains that some faults could have been active. The same applies to Figs. 8, 9, 10 described below.

The late Badenian–early Sarmatian (15–12.7 Ma) period was characterized by the lack of distinct regional tectonic stress changes. Extension was W–E to NW–SE oriented (Fig. 8) and this dominantly controlled the normal faulting. The σ_1 was vertical. Stress ellipsoids, calculated for locations 10, 16, 36, 78, 92, 109, 121, 122 and 123 (Table 1) have shapes close to the plane stress ones ($\sigma_1 > \sigma_2 > \sigma_3$). The σ_2

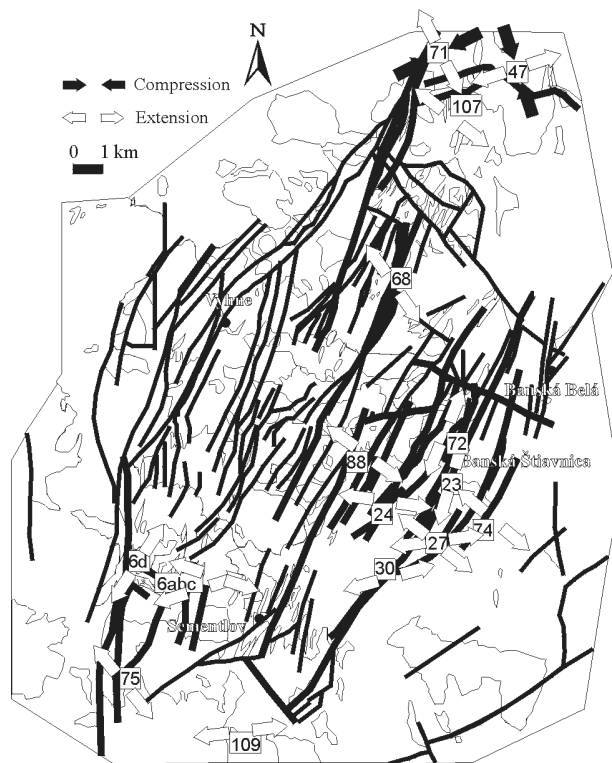
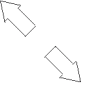
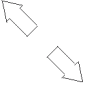
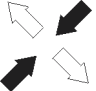
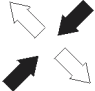

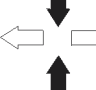


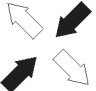
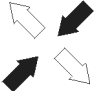



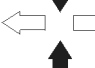
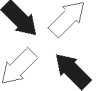
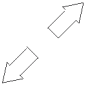


Fig. 7. Structural scheme of the central zone of the Štiavica stratovolcano (after Štol et al. 1990b) with paleostress configurations and faults determined as active during the early Badenian to earlier late Badenian. Divergent arrows indicate normal faulting, divergent arrows coupled with convergent ones indicate strike-slip regime. Arrows show the exact orientation of related principal stresses, unlike the Table 1.

Table 1: Paleostress configurations determined from rocks in the Banská Štiavnica area. Note that the table does not show the result of a tectonic event separation. It is a list of available stratigraphies with inventory of all paleostress configurations determined from these stratigraphies at related locations. The decrease of the number of paleostress configurations in younger stratigraphies is caused by the fact that they were deformed by a smaller number of tectonic events than older stratigraphies. Note that the orientations of paleostresses are generalized in order to demonstrate regional correlation. Codes S and H indicate the use of stress inversion software of Sperner et al. (1993) and Hardcastle & Hills (1991). The numbers in parentheses indicate the ratio of paleostress magnitudes. Divergent arrows indicate normal faulting, divergent arrows coupled with convergent ones indicate strike-slip regime.

Upper Sarmatian - Lower Panonian	Sarmatian
 4 (S), 113 (S), 116 (H, 0.1 e), 117 (H, 0.3 e)	 3 (S), 7 (S), 15 (H, 0.3 e), 40 (S), 77 (H, 0.2 e)
 114 (H, 0.2 e)	 40 (S)
 4 (S)	
 4 (S), 117 (H, 0.3 e), 119 (H, 0.8 e)	
Upper Badenian - Lower Sarmatian	Lower - early Upper Badenian
 10 (H, 0.4 e/ps), 70 (S), 78 (H, 0.5 ps), 80 (H, 0.3 e), 92 (H, 0.4 e/ps), 95 (H, 0.2 e), 120 (S), 121 (H, 0.4 e/ps), 122 (H, 0.4 e/ps)	 6a (S), 6b (S, H, 0.3 e), 16 (H, 0.5 ps), 20 (H, 0.2 e), 24a (S), 24b (H, 0.1 e), 27 (S), 36 (H, 0.6 ps), 64 (S), 68 (S), 69 (H, 0.2 e), 72 (S), 74 (H, 0.8 g), 75b (S), 75d (S), 83 (S), 84a (H, 0.2 e), 87 (S, H, 0.3 e), 88a (H, 0.8 g), 96 (S), 107 (H, 0.8 g)
 29 (S), 46 (S), 60 (S), 98 (S)	 71 (S), 84b (S)
 9 (S), 109 (H, 0.8 g), 123 (H, 0.4 e/ps)	 6c (S, H, 0.2 e), 27 (S), 30 (S), 55 (H, 0.2 e), 84b (S), 84d (S), 109 (H, 0.8 g)
 91 (S)	 47 (S)
 33 (S)	 6d (S), 23 (H, 0.2 e), 64 (H, 0.2 e), 72 (H, 0.2 e)

value is close to the mean of the remaining two. Locations 29, 33, 46, 60 and 98 indicate activity of the strike-slip faulting. The location 33 with NW-SE oriented compression and NE-SW extension (Table 1) is anomalous. It may indicate stress rotation inside a strike-slip fault zone as known from other regions (e.g. Bogen & Seeber 1986; Freund 1970, 1971, 1974; Nur et al. 1986; Ron et al. 1984; Scoti et al. 1991). Fig. 8 shows active faults of this period.

Stress magnitude calculation, using the stress ratio of Hardcastle & Hills (1991) (equal to 1-R ratio of Angelier 1989) $R = 0.4$ and $\psi = 0.0062893$, yields values of subvertical $\sigma_1 = 75.8$ MPa, subhorizontal $\sigma_2 = 45.7$ MPa and $\sigma_3 = 0.47$ MPa. The fast removal of the upper parts of the strato-volcanic cone above the intrusions (Fig. 2a-c) would remove roughly 42.5 MPa of the load during the late Badenian-early

Sarmatian. This would result in subhorizontal $\sigma_1 = 45.7$ MPa and $\sigma_3 = 0.47$ MPa and subvertical $\sigma_2 = 33.3$ MPa, changing the stress ellipsoid from the plane stress to an oblate one and exchanging σ_1 and σ_2 (locations 29, 46, 60, 98 in Fig. 8). Thus, the related kinematic regime changed from normal to strike-slip faulting. During the same time an emplacement of the granodiorite intrusion occurred.

Taking the density of the load (calculated proportionally to the content of lava flows, volcanoclastics and intrusives) to equal 2577 kgm^{-3} , the density of magma 2585 kgm^{-3} , s_{vertical} (load) 33.3 MPa and the magmatic pressure and intrusion height estimates mentioned earlier, the resulting magmatic pressure in the top of the intrusion by buoyancy calculation (Price & Cosgrove 1991) was about 37.7 MPa, nearly equal to the addition of s_{vertical} and the tensional strength of the sur-

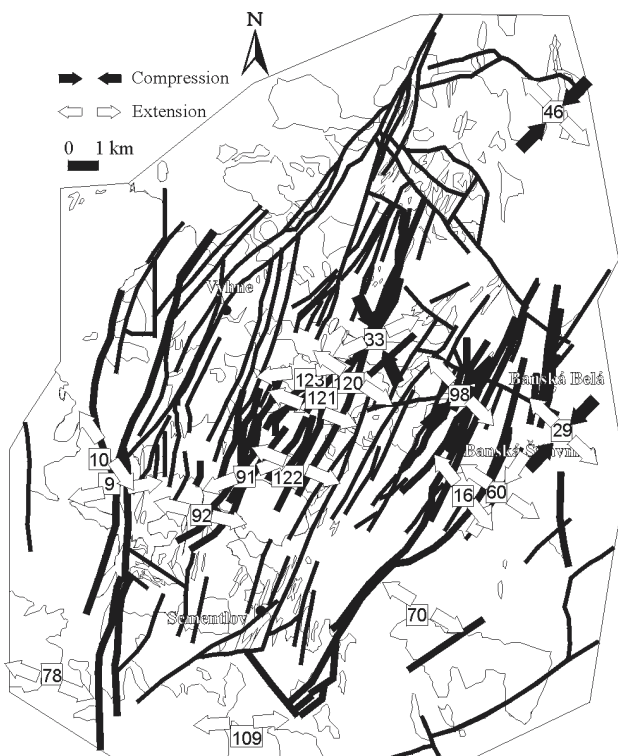


Fig. 8. Structural scheme of the central zone of the Štiavnica stratovolcano (after Štohl et al. 1990b) with paleostress configurations and faults determined as active during the late Badenian to early Sarmatian. For further explanations see Fig. 7.

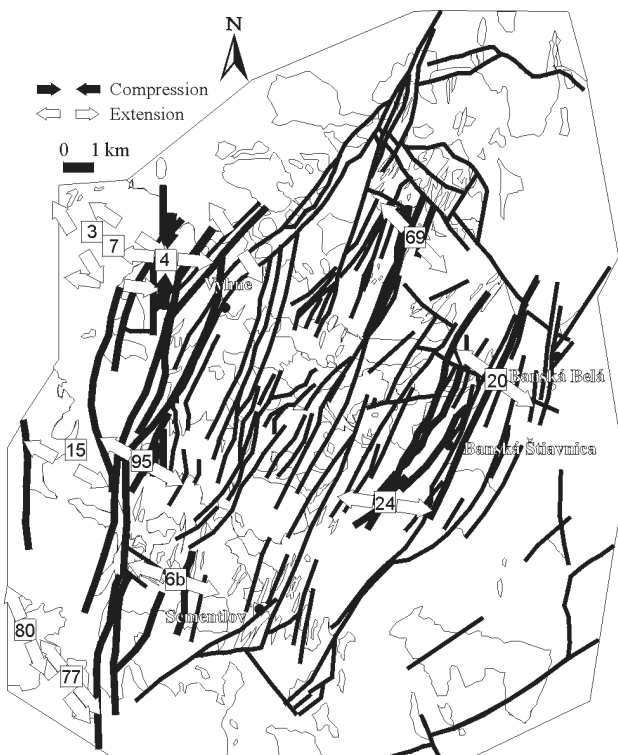


Fig. 9. Structural scheme of the central zone of the Štiavnica stratovolcano (after Štohl et al. 1990b) with paleostress configurations and faults determined as active during the Sarmatian. For further explanations see Fig. 7.

rounding rocks. Magmatic pressure further reduced the principal stresses in the surroundings of the intrusion and changed vertical $\sigma_2 = 33.3$ MPa to $\sigma_3 = -4.4$ MPa. Said differently, taking the determined tensile strength of the granodiorite = 2.5–4.9 MPa, the magmatic pressure was in most places larger than the sum of the vertical σ_3 and tensile strength. The change of subhorizontal $\sigma_1 = 45.7$ MPa and subhorizontal $\sigma_3 = 0.47$ MPa is neglectable, only σ_3 changes to σ_2 . The calculated effective subvertical extension was large enough to open a subhorizontal Svetozár-type vein system above the intrusion, that is in accordance with field evidence (e.g. Fig. 6a–c). The intrusion was fed for some time as indicated by the fact that: 1) subhorizontal veins underwent several overpressure cycles/episodes of reopening controlled by fluids escaping from the intrusion (Fig. 6f) and fluids were of magmatic origin, as shown by the isotopic data of Háber et al. (1994), 2) subhorizontal veins are cross cut by veins opened by tectonic W-E oriented extension, which are later cross cut by subhorizontal veins (Fig. 6d).

Previous calculations show that the hydrostatic stress state, which opened the anastomosing vein system (Fig. 6a–e), the oldest fracture system, could not have been created by tectonic stress/overburden removal stress/magmatic stress interplay. The calculated differential stress was too high to open fractures without a preferred orientation (see Cosgrove 1995 for details). The anastomosing vein system had to be opened by residual stress. It could be accumulated either by an abrupt temperature drop due to fast overburden removal (Fig. 2a–c) or by rather fast temperature drop during cooling and was independent of the stresses discussed above. Using the equations (4) and (5), the residual stress $\Delta\sigma_r$ would be larger than the strength of rock after the fast uplift of several tens of meters if there was no cooling of the intrusion. Taking cooling into account the uplift has to be larger. 0.5 % volume loss of the intrusion due to cooling would be large enough to generate this residual stress. However, there is a faster process of developing the residual stress available. Fig. 11a shows the modeled cooling T-t paths of points at various distances from the granodiorite intrusion/andesite country rock boundary. The most dramatic temperature changes, during the first 200,000 years after the intrusion, are recorded by the 1 km thick granodiorite and andesite zones at their boundary (Fig. 11b,c). Wherever fast cooling occurs over a temperature gradient of more than 35 °C, sufficient residual stress is built up to overcome the tensile strength of the rock (11d).

Later stages of the late Badenian–early Sarmatian (15–12.7 Ma) are characterized by the lack of distinct influence of either magmatic stress or overburden removal stress. The emplacement of quartz-diorite porphyry dykes (see Figs. 1, 3, 6b,c) postdates the granodiorite intrusion. Calculation of the average width and length of 128 dykes yields 1:5 ratio; 106 m:36 m. The dykes are inclined at angles of about 50–60° (Fig. 3), indicating that they are hybrid structures not formed by 100 % hydraulic fracturing (see Price & Cosgrove 1990). Their driving σ_1 – σ_3 stress difference is 19.6–24.5 MPa, i.e. 4T–5T, where T is the tensile strength of the rock. Taking the calculated value of σ_1 as roughly equal to 45.7 MPa, σ_3 becomes at least 4.3 times larger than the tensile strength of granodiorite. Fig. 3 shows that inclined dykes intruded upwards, experiencing decrease of the

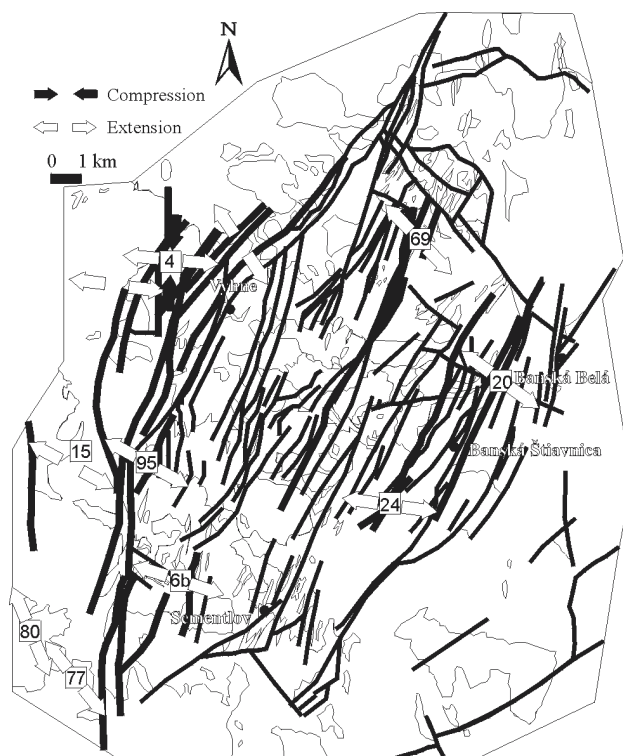


Fig. 10. Structural scheme of the central zone of the Štiavnica stratovolcano (after Štohl et al. 1990b) with paleostress configurations and faults determined as active during the late Sarmatian to early Pannonian. For further explanations see Fig. 7.

vertical load, until conditions for the formation of sills were met. At the junction of the dykes with sills, it has to be valid that $(\sigma_1 - \sigma_3) < (T_{\parallel} - T_{\perp})$, where T_{\parallel} is the strength of the host rock tested in the vertical direction and T_{\perp} is the strength of the host rock tested in the horizontal direction.

The Sarmatian (13.6–11.5 Ma) period was also characterized by W-E to NW-SE oriented extension (Fig. 9), which produced dominantly normal faulting. However, the stress ellipsoid shape, calculated for locations 6b, 15, 20, 24b, 69, 77, 80 and 95 (Table 1), changed to oblate, indicating progressively stronger regional extension. This is supported by the fact that there was not any significant erosion, except the local one of 400 m in the horst region (Háber et al. 1997), but rather the addition of new material on top of the pre-existing structures (Fig. 2e). It should change the ellipsoid to prolate, but the value of the R ratio decreased to indicate the oblate ellipsoid. Stress determined for location 40 shows the dextral strike-slip reactivation of suitably oriented faults. Fig. 9 shows active faults of this time period.

During the late Sarmatian–early Pannonian (12–10.7 Ma) period, the W-E to NW-SE oriented extension continued, later during the Pannonian it was replaced by N-S and E-W compression and extension, respectively (Fig. 10, Table 1). Late Sarmatian–early Pannonian stress ellipsoids calculated for locations 114, 116 and 117, with NW-SE oriented extension (Fig. 10, Table 1), have an oblate character, indicating strong regional extension. Subsequent fast erosion caused the σ_1/σ_2

exchange, reactivating pre-existing normal faults as strike-slip faults (location 4 in Fig. 10, 117 in Table 1). A younger stress pattern, resembling the present stress field (e.g. Gutdeutsch & Aric 1988), was determined from strike-slip faults at locations 4, 117 and 119. Fig. 10 shows active faults of this time period.

Interpretation

During the early Badenian–earlier late Badenian (16.5–15 Ma), the Štiavnica stratovolcano composed of andesite lava-, pyroclastic-, epiclastic flows and related sills and lacoliths formed (Fig. 2a). The volcanic cone underwent rather fast erosion. Synchronously, a quartz-diorite body was emplaced in its center, during the Badenian–early Sarmatian (15–12.7 Ma) (Fig. 2b). During the Badenian, the minimum horizontal stress σ_3 rotated clockwise roughly 90° from NE-SW to NW-SE (Table 1, Fig. 7). Denudation of the stratovolcano continued contemporaneously with the emplacement of the granodiorite body, 10 km in diameter and 7 km high (Fig. 2c). The rapid cooling experienced by the upper parts of the intrusion and adjacent zone of the andesite (Fig. 11) accumulated residual stress which opened an anastomosing pattern of fractures by hydraulic fracturing (Fig. 6a–e). The granodiorite body was not free to contract soon after releasing fluids due to its confinement provided by 2 mechanisms. The first one was the inhomogeneous cooling because the intrusion was welded to the country rock and the net temperature change was heterogeneous. The second one was imposed by the fact that granodiorite is a heterogeneous intergrowth of minerals of different thermal expansion coefficients and elastic contents.

The theoretical time-position zone of fracturation events (Fig. 11) does not fit the observation. The system of mineralized anastomosing tensional fractures seems to be present only in the outermost parts of the granodiorite and adjacent parts of the andesite. It implies that the fracturation took part during the earlier stages of the cooling and in the areas of the most dramatic temperature changes. The fracturation would be allowed during the small initial volume change due to the release of mineralized fluids. This would be further supported by the magmatic origin of the fluids recorded in these fractures, discussed earlier. It should be said that the modeling in Fig. 11 was done assuming no heat transfer by fluids, which makes the problem even more complex.

Removal of the overburden above the intrusion by the fast erosion interfered with the regional stress pattern changing the normal faulting regime driven by W-E to NW-SE oriented extension (Table 1, Fig. 7) to the strike-slip faulting regime. The input of magmatic stresses during the granodiorite emplacement affected the regional tectonic stress/overburden removal stress interplay, making σ_3 stress vertical. Magmatic pressure occasionally exceeded the sum of the σ_3 plus vertical strength. During related short time periods, this opened a subhorizontal Svetozár-type vein system cross-cutting the anastomosing vein system (Fig. 6a–c). The σ_3 stress become vertical few times as indicated by NE-SW oriented vertical veins cross-cutting subhorizontal veins and being cross-cut by younger subhorizontal veins (Fig. 6d). Later on, during the late Badenian–early Sar-

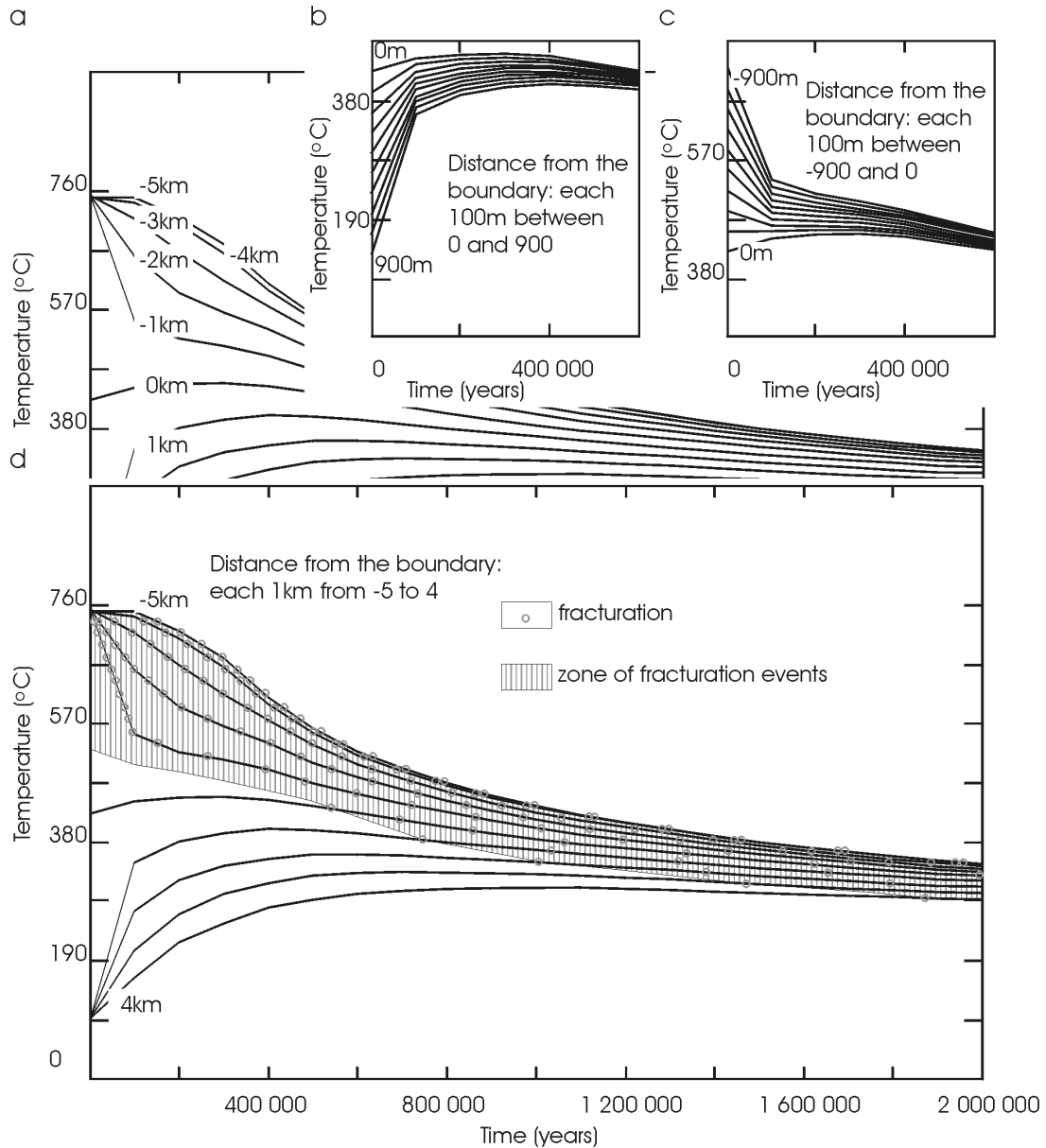


Fig. 11. (a) The T-t path diagram related to the cooling of the granodiorite intrusion. Each curve is made for a rock point localized at the specified distance from the intrusion/andesite country rock boundary. Explanation in text. (b-c) The same diagrams for the early stages of cooling around the intrusive contact. (d) Fracturation events triggered when the residual stress developed by the fast cooling overcomes the tensile strength of the host rock. Explanation in text.

matian (15–12.7 Ma), during the continuing denudation of the volcano, quartz-diorite porphyry sills and dykes were emplaced (Fig. 2e). Dykes pass to sills at the depth around the top of the granodiorite body, where the (σ_1 – σ_3) value meets the condition for sill formation, outlined earlier. Dense dyke spacing, general NE-SW trend and dyke dips around 60° indicate stronger NW-SE oriented regional tectonic extension, also indicated by paleostress calculations (Table 1). Lack of any ring and/or radial dykes does not support the collapse origin of the postulated caldera during the late Badenian–early Sarmatian.

Paleostress calculation also does not indicate the existence of strong vertical σ_1 stress and subhorizontal polydirectional

extension (Table 1). On the contrary, the subsiding central parts of the stratovolcano were controlled by faulting driven by regional W-E to NW-SE extension (Table 1, Fig. 8) and filled by sediment, tuffs, pyroclastic- and lava flows. The same stress configuration gained progressively stronger extension during the Sarmatian (13.6–11.5 Ma) (Table 1, Fig. 9). During this period, the horst structure developed in the central zone of the Štiavnica stratovolcano, synchronous with renewed andesite activity. The extension controlled NE-SW trending normal faults and extensional veins — migration paths of the base and precious metal mineralization fluids. Normal faults, dissecting any older structures, were

detached along the subhorizontal faults, which frequently utilized pre-existing subhorizontal veins. Fig. 6e shows an example of the boudinage related to such a reactivation. The distinct change of the stress configuration in the course of the Pannonian (11.5–6.2 Ma) reactivated pre-existing normal fault pattern as strike-slips (Fig. 10). This event is indicated by the occurrence of the youngest, ore deposits in the strike-slip related horse-tail structures at the southern ends of some pre-existing normal faults.

Discussion and conclusions

The data discussed in this paper indicate distinct regional tectonic stress changes during the Badenian (Table 1, Fig. 7). It was the period when the sinistral transpression characteristic for the NW boundary of the Inner Western Carpathians during the early Miocene changed to transtension. Areas located further towards the hinterland experience the clockwise rotation of the minimum and maximum horizontal stresses. The central zone of the Štiavnica stratovolcano experienced this rotation during the Badenian. This rotation in different areas has been suggested in numerous papers (e.g. Nemčok et al. 1989; Fodor et al. 1990; Csontos et al. 1991). The first and last stage of this rotation is also identified by Maťo et al. (1996) in the Rozália Mine.

The authors did not have sufficiently complete stratigraphy and sophisticated paleostress methods for a complete identification. This rotation caused the dextral reactivation of the pre-existing sinistral strike-slip in the area to the N of the Štiavnica stratovolcano (Kováč & Hok 1993) during the Badenian. Similar rotation, only relatively dated, was indicated by Sasvári & Schmidt (1994) in the Rozália Mine in Banská Hodruša.

The discussed clockwise σ_3 stress rotation can be dated to the middle-late Badenian by comparison with regional stress studies (e.g. Nemčok & Lexa 1990; Nemčok et al. 1993). The NW-SE oriented extension had to be already active during the late Badenian as indicated by the age of basal transgressive facies in the surrounding Turiec, Žiar Depressions and the Kremnica Graben, which were opened by this extension (e.g. Gašparík 1980, 1985; Gašparík et al. 1974; Konečný et al. 1983; Lexa et al. 1979, 1982). The same extension continued during the Sarmatian, as shown by the northern parts of the Turiec Depression where the Sarmatian sequence of the downthrown hanging wall thickens towards the normal fault, indicating its synsedimentary activity (Nemčok & Lexa 1990). These authors describe the same evidence from the Horná Nitra Depression. Sarmatian synsedimentary activity of the normal fault along the western margin of the Turiec Depression is indicated by coarse clastic horizons, abruptly pinching out in direction towards the basin (Gašparík 1985; Gašparík et al. 1974). The end of subsidence in these basins can be implied from the redeposited kaoline clay horizons in upper Pannonian and Pontian sediments of the Turiec Depression (Kraus 1986). This tectonic event was also recognized in the Rozália Mine by Maťo et al. (1996). The authors also distinguished a strike-slip event, which is not dated, so it is difficult to discuss its unexpected regime.

Another interesting problem is the evolution of the stress configuration comprising NW-SE oriented extension. This became progressively more oblate in character during the Sarmatian (Table 1). This indicates a progressively stronger regional tectonic extension. If this stress configuration is driven by plate movements, the timing and orientation of these extensional events should be in accordance with the timing and orientation of thrust movements recorded in the Outer East-Carpathian accretionary wedge. They are in accordance, because this is the time when the thrusting in the Outer Western Carpathians ceased (e.g. Buday 1965; Jurková 1971; Vass et al. 1983; Książkiewicz 1960) and remained active only in the Outer Eastern Carpathians during the Sarmatian and late Sarmatian–early Pannonian (e.g. Vialov 1974; Saulea 1969, Jiříček 1979), which should increase the NW-SE extension in the hinterland.

It is interesting to note that no structural evidence has been found for collapse along the caldera fault. There are no circular and radial dyke intersections with the surface, which would indicate a prolate stress with vertical maximum compression and polydirectional subhorizontal extension. The caldera fault was specially studied in the field and none of the locations in its vicinity provide Late Badenian–early Sarmatian paleostress indicating either gravity collapse or vertical tension (Table 1, Fig. 7), unlike, for example the stresses determined at Sierra Negra volcano, Galapagos (Reynolds et al. 1995). Gravity collapse would have been proved by a stress ratio R equal to 0.9, that is nearly uniaxial compression and perpendicular polydirectional extension.

During the early Badenian–earlier late Badenian (16.5–15 Ma), the minimum horizontal stress σ_3 rotated clockwise roughly 90° from the NE-SW to NW-SE orientation. Denudation of the stratovolcano started earlier in this time period and continued contemporaneously with the emplacement of the granodiorite body. The rapid cooling of the upper parts of the granodiorite intrusion accumulated residual stress which opened the anastomosing vein pattern (Fig. 6a–e). The interplay between the erosional overburden removal from above the intrusion and the regional stress changed the normal faulting regime to the strike-slip faulting one, both driven by W-E to NW-SE oriented extension (Table 1, Fig. 7). Magmatic stresses during the granodiorite emplacement interfered with both regional tectonic stress and overburden removal stress, making σ_3 stress vertical and controlling the development of subhorizontal veins in the areas where the sum of σ_3 plus host rock strength was exceeded (Fig. 6a–c).

During the late Badenian–early Sarmatian (15–12.7 Ma), N-S to NNE-SSW striking faults were reactivated as dextral strike-slip faults, NE-SW ones as normal faults by the stress comprising NW-SE extension (Fig. 8). Normal faults and extensional bridges along the strike-slip faults were the places of the ore deposition.

The same stress configuration gained progressively stronger extension during the Sarmatian (13.6–11.5 Ma) (Table 1). During this period, the horst structure developed in the central zone of the Štiavnica stratovolcano. Normal faulting along N-S to NE-SW trending faults was dominant in the central zone of the Štiavnica stratovolcano (Fig. 12) and was the place of the ore deposition.

A distinct change of the stress configuration happened during the Pannonian (11.5–6.2 Ma) (Table 1, Fig. 10). Pre-existing NE-SW normal faults were reactivated as sinistral strike-slip faults (Fig. 10). Their extensional bridges were the place of the ore deposition.

Acknowledgements: The follow-up work of MN, after the end of the Slovak Geol. Survey Project, has been carried under the financial support of the Lise Meitner Fund, Austria, later by the Alexander von Humboldt Fund. Authors are grateful for rock mechanics tests made by L. Sterba and S. Urban. This paper benefited from the help with field work and discussions with J. Lexa, D. Onáčila, J.-P. Petit, J. Štohl, V. Konečný, R. Gazdik and number of other people. The observations shown in Fig. 6 were made during a short field trip with J. Lexa and J. Štohl. We thank L. Fodor, K. Schulmann, J. Cosgrove and anonymous reviewers whose comments improved the paper.

References

- Anderson J.L. & Smith D.R. 1995: The effects of temperature and CO₂ on the Al-in-hornblende barometer. *Amer. Mineralogist* 80, 245–254.
- Angelier J. 1989: From orientation to magnitudes in paleostress determinations using fault slip data. *J. Struct. Geol.* 11, 37–50.
- Bergerat F. 1989: From pull-apart to the rifting process: the deformation of the Pannonian basin. *Tectonophysics* 157, 271–280.
- Blundy D.J. & Holland T.J.B. 1990: Calcic plagioclase equilibria and new amphibole-plagioclase geothermometer. *Contr. Mineral. Petrology* 104, 208–224.
- Bogen N.L. & Seeber L. 1986: Neotectonics of rotating blocks within the San Jacinto fault zone, southern California (abs). *EOS* 67, 1200.
- Buday T. 1965: Die Tektonogenese und der Bau der Neogenen Becken der Westkarpaten. In: Buday T., Cicha I. & Seneš J. (Eds.): *Miozän der Westkarpaten*. GÚDŠ, Bratislava, 169–250.
- Cermak V. & Rybach L. 1982: Thermal conductivity and specific heat of minerals and rocks. In: Angenheister G. (Ed.): *Landolt-Bornstein Numerical Data and Functional Relationships in Sci. and Technol., New Ser., Group V* 16. Springer-Verlag, Berlin.
- Cloetingh S.A.P.L., Zoetemeijer R. & van Wees J.D. 1995: Tectonics I. Tectonics and basin formation in convergent settings; thermo-mechanical evolution of the lithosphere and basin evolution in compressive tectonic regimes. *Short Course*, Vrije University, Amsterdam.
- Cosgrove J.W. 1995. The expression of hydraulic fracturing in rocks and sediments. In: Ameen M.S. (Ed.): *Fractography: fracture topography as a tool in fracture mechanics and stress analysis*. *Geol. Soc. Spec. Publ.* 92, 187–196.
- Csontos L., Tari G., Bergerat F. & Fodor L. 1991: Evolution of the stress field in the Carpatho-Pannonian area during the Neogene. *Tectonophysics* 199, 73–92.
- Csontos L., Nagymarosy A., Horváth F. & Kováč M. 1992: Tertiary evolution of the intracarpathian area: a model. *Tectonophysics* 208, 221–241.
- Fodor L., Marko F. & Nemčok M. 1990: Evolution microtectonique et paléochamps de contraintes du Bassin de Vienne. *Geod. Acta* 4, 147–158.
- Freund R. 1970: Rotation of strike-slip faults in Sistan, southeast Iran. *J. Geol.* 78, 188–200.
- Freund R. 1971: The Hope fault, a strike-slip fault in New Zealand. *N. Z. Geol. Surv. Bull.* 86, 1–49.
- Freund R. 1974: Kinematics of transform and transcurrent faults. *Tectonophysics* 21, 93–134.
- Gašparik J. 1980: Geological evaluation of southern part of Turčianska kotlina Depression. *Report*, archive GÚDŠ Bratislava (in Slovak).
- Gašparik J. 1985: Basic features of geological structure of Hornonitrianska and Turčianska kotlina depressions. In: Samuel O. & Franko O. (Eds.): *Spríevodca ku XXV. celoštátnemu zjazdu slovenskej geologickej spoločnosti*. GÚDŠ, Bratislava, 53–56 (in Slovak).
- Gašparik J. et al. 1974: Structural borehole GHŠ-1 (Horná Štubňa). *Reg. Geológia Západ. Karpát*, 3 (in Slovak).
- Gutdeutsch R. & Aric K. 1988: Seismicity and neotectonics of the East Alpine-Carpathian and Pannonian area. In: Royden L.H. & Horváth F. (Eds.): *The Pannonian Basin: A Study of Basin Evolution*. AAPG Memoir 45, 183–194.
- Háber M., Jeleň S., Maťo L. & Kovalenker V.A. 1997: Modelling of mineral-forming processes at the Banská Štiavnica epithermal deposit (Western Carpathians, Slovak Republic). Proceedings of the 9th IAGOD Symposium, Beijing, China, August 12–18 1994, *E. Schweizerbart'sche Verlagsbuchhandlung*, Stuttgart, 21.
- Hammarstrom J.M. & Zen E. 1986: Aluminium in hornblende: an empirical igneous geobarometer. *Amer. Mineralogist* 71, 1297–1313.
- Hardcastle K.C. 1989: Possible paleostress tensor configurations derived from fault-slip data in eastern Vermont and western New Hampshire. *Tectonics* 8, 265–284.
- Hardcastle K.C. & Hills L.S. 1991: BRUTE3 and SELECT. Quick-basic 4 programs for determination of stress tensor configurations and separation of heterogeneous populations of fault-slip data. *Comput. & Geosci.* 17, 23–43.
- Hollister L.S., Grisson G.C., Peters E.K., Stowell H.H. & Sisson V.D. 1987: Confirmation of the empirical correlation of Al in hornblende with pressure of solidification of calc-alkaline plutons. *Amer. Mineralogist* 72, 231–239.
- Ibrmajer J. et al. (Ed.) 1989: Geophysical picture of ČSSR. *UUG Praha*.
- Jaeger J.C. & Cook N.G.W. 1976: Fundamentals of rock mechanics. *J. Wiley & Sons*, New York.
- Jiríček R. 1979. Tectogenetic development of the Carpathian arc in the Oligocene and Neogene. In: Mahel M. (Ed.): *Tectonic Profiles of the West Carpathians*. GÚDŠ, Bratislava, 203–214 (in Czech, English summary).
- Johnson M.C. & Rutherford M.J. 1988: Experimental calibration of an aluminium in hornblende geobarometer applicable to calc-alkaline rocks. *EOS* 69, 1511.
- Jurková A. 1971: Die Entwicklung der Badener vortiefe im Raum der Mährischen Peorte und Gebiet von Ostrava (eine Rekonstruktion auf Grund des Studiums des Begraben Paläozoikum und dessen Neoiden deckgebirges). *Geol. Práce, Spr.* 57, 155–160 (in Slovak, German résumé).
- Kantor J. & Ďurkovičová J. 1985: Genetical characteristics of selected mineralizations in the Western Carpathians. *Report*, archive GÚDŠ, Bratislava (in Slovak).
- Kantor J., Ďurkovičová J., Eliáš K., Repčok I., Ferenčíková E., Hasková A., Kvarová A., Růčka I. & Sladková M. 1988: Isotopic research of metallogenic processes. Part I: Rudno-Brehy-Pukanec area. *Report*, archive GÚDŠ, Bratislava (in Slovak).
- Konečný V. & Lexa J. 1984: Regional geological maps of Slovakia: Geological map of the Central Slovakia Neogene Volcanic Field. Scale 1:100,000. GÚDŠ, Bratislava.
- Konečný V., Lexa J. & Planderová E. 1983: Stratigraphy of the

- Central Slovakia, Volcanic field. *Západ. Karpaty, Sér. Geol.* 9, 1–203 (in Slovak, English abstract and summary).
- Kováč P. & Hók J. 1993: The Central Slovak fault system — the field evidence of a strike-slip. *Geol. Carpathica* 44, 3, 155–159.
- Kraus I. 1986: Kaolins and kaolinite clays of the Western Carpathians: geologic-depositional conditions, mineralogical composition, genesis and age. *DrSc Thesis*, University Comeniana, Bratislava (in Slovak).
- Książkiewicz M. 1960: Zarys paleografii polskich Karpat fliszowych. *Práce Inst. Geol.* 33, 209–231.
- Lexa J. et al. 1979: Evaluation of the structural borehole LX-5 (Kremnica). *Report*, archive GÚDŠ, Bratislava (in Slovak).
- Lexa J. et al. 1982: Explanations to the sheets 36–132 (H. Štubňa) and 36–134 (Kremnica). *Report*, archive GÚDŠ, Bratislava (in Slovak).
- Lexa J. & Konečný V. 1974: The Carpathian volcanic arc: A discussion. *Acta. Geol. Acad. Sci. Hung.* 18, 279–293.
- Lexa J., Konečný V., Kaličiak M. & Hojstrícová V. 1993: Distribution of volcanites of Carpatho-Pannonian region in time-space. In: Rakús M. & Vozár J. (Eds.): *Geodynamical model and deep structure of the Western Carpathians*. GÚDŠ, Bratislava, 57–69 (in Slovak).
- Lexa J., Štohl J. & Konečný V. 1999: Banská Štiavnica ore district: relationship among metallogenetic processes and the geological evolution of a stratovolcano. *Mineralium Deposita* 34, 639–654.
- Linzer H.G., Ratschbacher L. & Frisch W. 1995: Transpressional collision structures in the upper crust: the fold-thrust belt of the Northern Calcareous Alps. *Tectonophysics* 242, 41–61.
- Maťo L., Sasvári T., Bebej J., Kraus I., Schmidt R. & Kalinaj M. 1996: Structurally-controlled vein-hosted mesothermal gold-quartz and epithermal precious and base metal mineralization in the Banská Hodruša ore field, Central Slovakia neovolcanites. *Miner. Slovaca* 28, 455–490 (in Slovak, English abstract and summary).
- Nemčok M., Hók J., Kováč P., Marko F., Madarás J. & Bezák V. 1993: Tertiary tectonics in the Western Carpathians. In: Rakús M. & Vozár J. (Eds.): *Geodynamical model and deep structure of the Western Carpathians*. GÚDŠ, Bratislava, 263–267 (in Slovak).
- Nemčok M. & Lexa J. 1990: Evolution of the basin and range structure around the Žiar mountain range. *Geol. Zbor. Geol. Carpath.* 41, 3, 229–258.
- Nemčok M. & Lexa J. 1995: Structural analysis of the central zone of the Štiavnica stratovolcano in relation to the development of vein structures. *Report*, archive GÚDŠ (in Slovak).
- Nemčok M., Marko F., Kováč M. & Fodor L. 1989: Neogene tectonic and paleostress changes in the Czechoslovak part of the Vienna Basin. *Jb. Geol. B.-A.* 132, 2, 443–458.
- Nur A., Ron H. & Scotti O. 1986: Fault mechanics and the kinematics of block rotations. *Geology* 14, 746–749.
- Peacock S.M. 1990: Computer Exercises for Numerical Simulation of Metamorphic P-T-t paths. *Short Course*, Arizona State University, Tempe, 1–189.
- Pécskay Z., Lexa J., Szakács A., Balogh K., Seghedi I., Konečný V., Kovacs M., Márton E., Kaličiak M., Széky-Fux V., Póka T., Gyarmati P., Edelstein O., Rosu E. & Zec B. 1995: Space and time distribution of Neogene-Quaternary volcanism in the Carpatho-Pannonian region. In: Downes H. & Vaselli O. (Eds.): *Neogene and related magmatism in the Carpatho-Pannonian region*. *Acta Vulcanol.* 7, 2, 15–28.
- Piwinski A.J. 1975: Experimental studies of granitoid rocks near the San Andreas fault zone in the Coast and Transverse Ranges and Mojave Desert, California. *Tectonophysics* 25, 217–231.
- Póka T. 1988: Neogene and Quaternary volcanism of the Carpathian-Pannonian region: changes in chemical composition and its relationship to basin formation. In: Royden L.H. & Horváth F. (Eds.): *The Pannonian Basin. A study in basin evolution*. *AAPG Mem.* 45, 257–276.
- Price N.J. & Cosgrove J.W. 1991: Analysis of Geological Structures. *Cambridge University Press*, 1–502.
- Ramsay J.G. & Huber M.I. 1983: The techniques of modern structural geology. Volume I. *Academic Press*, London, 1–307.
- Ratschbacher L., Frisch W. & Linzer H.G. 1991a: Lateral extrusion in the Eastern Alps, part 2: structural analysis. *Tectonics* 10, 2, 257–271.
- Ratschbacher L., Merle O., Davy P. & Cobbold P. 1991b: Lateral extrusion in the Eastern Alps, part 1: boundary conditions and experiments scaled for gravity. *Tectonics* 10, 2, 245–256.
- Reynolds R.W., Geist D. & Kurz M.D. 1995: Physical volcanology and structural development of Sierra Negra volcano, Isabela Island, Galapagos archipelago. *GSA Bull.* 107, 1398–1410.
- Ron H., Freund R. & Garfunkel Z. 1984: Block rotation by strike-slip faulting: structural and paleomagnetic evidence. *J. Geophys. Res.* 89, 6 256–6 270.
- Royden L.H. & Báldi T. 1988: Early Cenozoic tectonics and paleogeography of the Pannonian and surrounding regions. In: Royden L.H. & Horváth F. (Eds.): *The Pannonian Basin. A study in basin evolution*. *AAPG Mem.* 45, 1–16.
- Royden L.H., Horváth F. & Burchfiel B.C. 1982: Transform faulting, extension and subduction in the Carpathian-Pannonian region. *Geol. Soc. Amer. Bull.* 73, 717–725.
- Royden L.H., Horváth F., Nagymarosy A. & Stegena L. 1983: Evolution of the Pannonian basin system. 2. Subsidence and thermal history. *Tectonics* 2, 91–137.
- Royden L.H., Horváth F. & Rumpel J. 1993: Evolution of the Pannonian basin system. 1. Tectonics. *Tectonics* 2, 63–90.
- Salters J.M., Hart S.R. & Panto G. 1988: Origin of late Cenozoic volcanic rocks of the Carpathian arc, Hungary. In: Royden L.H. & Horváth F. (Eds.): *The Pannonian Basin. A study in basin evolution*. *AAPG Mem.* 45, 279–292.
- Săndulescu M. 1988: Cenozoic tectonic history of the Carpathians. In: Royden L.H. & Horváth F. (Eds.): *The Pannonian Basin. A study in basin evolution*. *AAPG Mem.* 45, 17–26.
- Sasvári T. & Schmidt R. 1994: Some results of the structural-geological evaluation of Svetozár vein, 16th level, Rozália mine, Banská Hodruša. In: *Proceedings of the Conference "The latest knowledge from investigation, exploration, exploitation and treatment of precious ores in Slovakia"*, 1. July 1994, Hodruša-Hámre, 58–71 (in Slovak).
- Saulea E. 1969: Atlas litofacial. VI. Neogen. From: Jiříček 1979. Tectonical development of Carpathian arc in Oligocene and Neogene. In: Maheľ M. (Ed.): *Tectonic profiles in the West Carpathians*. GÚDŠ, Bratislava, 205–215 (in Slovak).
- Scoti O., Nur A. & Estevez R. 1991: Distributed deformation and block rotation in three dimensions. *J. Geophys. Res.* 96, 12 225–12 243.
- Schmidt M.W. 1992: Amphibole composition in tonalite as a function of pressure: an experimental calibration of the Al-in-hornblende barometer. *Contr. Mineral. Petrology* 110, 304–310.
- Sperner B., Ratschbacher L. & Ott R. 1993: Fault-striae analysis: a TURBO PASCAL program package for graphical presentation and reduced stress tensor calculation. *Comput. & Geosci.* 19, 1361–1388.
- Stegena L., Geczy B. & Horváth F. 1975: Late Cenozoic Evolution of the Pannonian Basin. *Tectonophysics* 26, 71–91.
- Suppe J. 1985: Principles of Structural Geology. *Prentice-Hall, Inc., Englewood Cliffs* 1–537.
- Šefara J. et al. 1976: Geophysical research of the Central Slovak neovolcanite basement. *Report*, archive of Geofond Bratislava,

- 1–241 (in Slovak).
- Štohl J., Hojstričová V., Lexa J., Rojkovičová L., Žáková E., Gargulak M., Stana S., Kantor J. & Ďurkovičová J. 1990a: Final report — borehole B-1/2000 Horná Roven. *Report*, archive GÚDŠ, Bratislava (in Slovak).
- Štohl J., Lexa J., Konečný V., Marsina K., Hojstričová E., Rojkovičová L., Mihaliková A., Hók J., Kacer S., Vozár J. & Konečný P. 1990b: Evaluation of Cu, Pb-Zn and Au-Ag prognosticated ore sources of the central zone of the Štiavnica stratovolcano. *Report*, archive GÚDŠ, Bratislava (in Slovak).
- Tschernyshev I.V., Háber M., Kovalenker V.A., Ivanenko V.V., Jeleň S. & Karpenko M.I. 1995: To the age position of the magmatic events and epithermal Au-Ag-base metals mineralisation in the central zone of the Banská Štiavnica stratovolcano: K-Ar data. *Geol. Carpathica* 46, 327–334.
- Turner F.J. 1953: Nature and dynamic interpretation of deformation lamellae in calcite of three marbles. *Amer. J. Sci.* 251, 276–298.
- Vass D., Krystek I. & Stráník Z. 1983: Tectonic activity in time of formation of Main and Late molasses in Czechoslovakian West Carpathians. In: *Contributions on geological development of molasses in some regions of Europe and U.S.S.R. and on block tectonics of Elbe-Lineament*. Central Inst. for Physics of the Earth, Potsdam.
- Vialov O. 1974: Transcarpathian depression. In: Maheľ M. (Ed.): *Tectonics of the Carpathian-Balkan Regions*. GÚDŠ, Bratislava, 203–205.